Numerical simulation of crack formation due to desiccation in clay surface

DENG Gang[1], SHEN Zhu-jiang[1, 2], YANG Dai-quan[2, 3]

(1. Department of Hydraulic Engineering, Tsinghua University, Beijing 100084, China; 2. Nanjing Hydraulic Research Institute, Nanjing 210024, China; 3. Amberg & TTI Engineering Pte Ltd, Singapore 449269, Singapore)

Abstract: A simplified consolidation theory for unsaturated soils was proposed based on an assumption that pore air pressure equaled to the atmosphere pressure. A finite element computer program for saturated soils was revised accordingly in order to be used in the analysis of crack formation and propagation upon drying on the clay surface. In numerical simulation, the distribution of polygonal cracks was simplified as an axisymmetrical problem with a double hardening elasto-plastic model adopted for soil skeleton. The sensitivities of various parameters to the width and depth of cracks developed were also studied.

Key words: numerical simulation; shrinkage crack; clay; consolidation theory of unsaturated soils

CLC number: TU44 **Document code**: A **Article ID**: 1000－4548(2006)02－0241－08

Biography: DENG Gang(1979－), Ph. D. Candidate. He has been engaged in: numerical simulation of geomechanics and geoengineering phoblems, safety evaluation of structures and geotechnical buildings.

粘土表面干缩裂缝形成过程的数值模拟

邓 刚[1]，沈珠江[1, 2]，杨代泉[2, 3]

（1. 清华大学水利水电工程系，北京 100084；2. 南京水利科学研究院，江苏 南京 210024；
3. Amberg & TTI Engineering Pte Ltd, Singapore 449269）

摘 要：基于孔隙气压力等于大气压力的假定，建议了针对非饱和土的简化固结理论。相应的修改了饱和土的有限元程序，用于分析粘土表面干缩裂缝的形成过程。数值分析中将多边形网状分布的裂缝简化为轴对称问题，对土骨架采用弹塑性的双硬化模型进行描述，并分析了不同参数对裂缝宽度和深度影响的敏感性。

关键词：数值模拟；干缩裂缝；粘土；非饱和土固结理论

0 Introduction

It is natural phenomena that shrinkage cracks occur on clay surface upon drying during dehydration period, which often become main seepage path eventually. Because of cracks, softening of sopped clays and initiation of landslide are therefore activated. And the diffusion of pollutant along the cracks may also speed up. The formation of cracks often results in failure of slope or pollution to environment sometime. It is of importance to study this problem but very few investigations have been carried out so far. The most research work was limited to one-dimensional infiltration (Morris P H[1], 1992; Abu-Hejleh A N, et al[2], 1995; Konrad J M, et al[3], 1997). Even if the study object is limited to be a flat ground, the seepage and displacement within this ground are certainly to be three-dimensional problem in the event of that the cracks are developed. In fact, formation of cracks is a typical problem with strain localization. Therefore, it has to be the only way to study this problem with three-dimensional displacement and seepage coupled analysis which is based on the theory of strain localization.

Fracture mechanics has prevailed in crack analysis of solid material. It is common to implement fracture mechanics in cracking analysis of soils (Konrad J M, et al[3], 1997; Lee F H, et al[4], 1998; LI Hong-sheng et al.[5], 2002). But the room for applying fracture mechanics to soil mechanics is limited. Firstly, fracture mechanics is proposed based on the concept of homogeneous medium, which does not apply to non-homogeneous material like soils. Secondly, study objects of fracture mechanics are subsistent cracks. What problems can fracture mechanics resolve is not how cracks are going to be initialized, but how the existing cracks extend and develop. Some scholars proposed cracking criterion with an assumption

Received date: 2005－05－19

that tension stress equals to tensile strength, and a proposal of another parameter called critical strain energy release rate to estimate the propagation of cracks (Konrad J M, et al[3], 1997; Lee F H, et al[4], 1998). Proposal of the so-called critical strain energy release rate is not helpful because crack developing is determined naturally by release and transfer of tensile stress. As the cracks develop with depth, effective stresses will increase due to the self-weight of soil. Therefore the cracking will stop eventually. To be beard in mind that cracking in soil is totally different from those in solid materials where the crack can cut through the whole component. In terms of the point of view for fracture mechanics, there is stress concentration on crack tip which should be taken into consideration. To handle the stress concentration, special measures including distinct shape function or high density mesh near the crack tip should be adopted in the finite element analysis. With consideration of the actual distribution of surface crack in soil which is often irregular polygon, and referring to the method in sand drain analysis, the authors choose a representative polygonal prism and simplify it into an axisymmetric problem in order to perform finite element numerical simulation and investigate the influence of soil characteristics on the development of crack depth and crack spacing upon drying.

1 Simplified consolidation theory for unsaturated soils

As any soil including saturated soil will turn into unsaturated soil or further develop its unsaturated status upon drying, a consolidation theory for unsaturated soils shall therefore be implemented for analysis of shrinkage cracking due to drying in the soils. The simplified consolidation theory proposed for the deformation analysis of channel slope of unsaturated expansive soils by Shen Z J[6] (1996), in which the pore air pressure was assumed to be equal to the atmosphere pressure, is modified as discussed in the following in order to simulate shrinkage cracking due to drying in the soils.

1.1 Reduced suction and effective stress

Let $\sigma_m=(\sigma_1+\sigma_2+\sigma_3)/3$ be average stress or spherical stress, u_a and u_w be pore air pressure and pore water pressure, respectively. Then the volumetric change caused by spherical stress can be expressed as follows:

$$\Delta\varepsilon_v = m(\Delta\sigma_m - \Delta u_a) + m_b(\Delta u_a - \Delta u_w) \quad , \tag{1}$$

where m and m_b are two compression coefficients. Reduced suction can be defined as

$$\bar{s} = \int \chi(\Delta u_a - \Delta u_w) \quad , \tag{2}$$

where $\chi = m_b/m$. Taking into consideration of Eq. (2), Eq. (1) can be simplified as

$$\Delta\varepsilon_v = m\Delta\sigma_m' \quad , \tag{3}$$

where

$$\Delta\sigma_m' = \Delta\sigma_m - \Delta u_a + \Delta\bar{s} \quad , \tag{4}$$

is increment effective stress. If the effective stress is regarded as a state variable, which has effect on deformation, the integrability of Eq.(2) must be satisfied. This simply means that the coefficient χ should be a function of suction (u_a–u_w).

In view of the research findings on the effective stress in association with shear strength, it has been proved by many researchers that the coefficient χ is probably only the function of degree of saturation (Jiang Pengnian[7], 1989). There has still been little progress in research on the effective stress in association with deformation so far. Nevertheless, it is quite sure that the coefficient χ should be a function of suction (u_a–u_w) under monotonous loading and monotonous drying conditions. For this reason, the concept of effective stress for unsaturated soils is therefore introduced for the following discussion.

If pore air pressure is assumed to be equal to zero, reduced suction and effective stress can be simplified as follows

$$\sigma_m' = \sigma_m + \bar{s} \quad , \tag{5}$$

and

$$\bar{s} = -\bar{u}_w = -\bar{\chi}u_w \quad , \tag{6}$$

where

$$\bar{\chi} = \frac{\int \chi \Delta u_w}{u_w} \quad , \tag{7}$$

and $\bar{u}_w$ is the so-called reduced pore pressure. On the basis of the aforementioned discussion, the stress-strain relationships of unsaturated soils can be generally expressed as

$$\{\Delta\varepsilon\} = [C](\{\Delta\sigma\} - \Delta\bar{u}_w\{I\}) \quad , \tag{8}$$

where $[C]$ is the flexibility matrix, and $\{I\} = \{111000\}^T$ is the unit tensor.

1.2 Equilibrium equations for forces

The stress-strain relationship for axisymmetric problem can be expressed as follows

$$\begin{Bmatrix}\Delta\sigma_r\\ \Delta\sigma_z\\ \Delta\sigma_\theta\\ \Delta\tau_{rz}\end{Bmatrix}=\begin{bmatrix}d_{11}\ d_{12}\ d_{13}\ d_{14}\\ d_{21}\ d_{22}\ d_{23}\ d_{24}\\ d_{31}\ d_{32}\ d_{33}\ d_{34}\\ d_{41}\ d_{42}\ d_{43}\ d_{44}\end{bmatrix}\begin{Bmatrix}\Delta\varepsilon_r\\ \Delta\varepsilon_z\\ \Delta\varepsilon_\theta\\ \Delta r_{rz}\end{Bmatrix}+\begin{Bmatrix}\Delta\bar{u}_w\\ \Delta\bar{u}_w\\ \Delta\bar{u}_w\\ 0\end{Bmatrix} \quad , \tag{9}$$

where r and z are the radial coordinate and vertical coordinate, respectively (Positive direction of z coordinate represents upwards). If u_r, u_z and $\bar{u}_w$ are three fundamental variables, applying Eq. (9) to force equilibrium equations will yield

$$d_{11}\frac{\partial^2\Delta u_r}{\partial r^2}+(d_{14}+d_{41})\frac{\partial^2\Delta u_r}{\partial r\partial z}+d_{44}\frac{\partial^2\Delta u_r}{\partial z^2}+d_{13}\frac{\partial\Delta u_r}{r\partial r}+$$
$$d_{34}\frac{\partial\Delta u_r}{r\partial z}-d_{33}\frac{\Delta u_r}{r^2}+d_{14}\frac{\partial^2\Delta u_z}{\partial r^2}+(d_{12}+d_{44})\frac{\partial^2\Delta u_z}{\partial r\partial z}+$$
$$d_{42}\frac{\partial^2\Delta u_z}{\partial z^2}+d_{34}\frac{\partial\Delta u_z}{r\partial r}+d_{32}\frac{\partial\Delta u_z}{r\partial z}-\frac{\partial\Delta\bar{u}_w}{\partial r}=\Delta F_r \quad , \tag{10a}$$

$$d_{41}\frac{\partial^2\Delta u_r}{\partial r^2}+(d_{21}+d_{44})\frac{\partial^2\Delta u_r}{\partial r\partial z}+d_{24}\frac{\partial^2\Delta u_r}{\partial z^2}+d_{43}\frac{\partial\Delta u_r}{r\partial r}+d_{23}\frac{\partial\Delta u_r}{r\partial z}+$$
$$d_{44}\frac{\partial^2\Delta u_z}{\partial r^2}+(d_{24}+d_{42})\frac{\partial^2\Delta u_z}{\partial r\partial z}+d_{22}\frac{\partial^2\Delta u_z}{\partial z^2}-\frac{\partial\Delta\bar{u}_w}{\partial z}=\Delta F_z \quad , \tag{10b}$$

where ΔF_r and ΔF_z are the load increments in radial and vertical directions, respectively.

1.3 Continuity equations for pore water phase

If v_w denotes the volume occupied by the pore water, and the degree of saturation is defined by $S_r=v_w/e$, where e is the void ratio, then the continuity equations for the pore water can be expressed as

$$\frac{\partial\varepsilon_v}{\partial t}=\frac{1}{e}\frac{\partial v_w}{\partial t}-S_r\frac{\partial e}{\partial t} \quad , \tag{11}$$

Taking into account that $\mathrm{d}e/(1+e)=-\mathrm{d}\varepsilon_v$, $e/(1+e)=n$ and $1/(1+e)\cdot\mathrm{d}v_w/\mathrm{d}t=-\mathrm{div}(\vec{q})$, and assuming that relationship between S_r and $-u_w$ (soil-water characteristic equations) has been measured and converted into following format:

$$S_r=f(-\bar{u}_w) \quad , \tag{12}$$

therefore the following equation can be obtained by dividing Eq. (11) by (1+e):

$$\mu n\frac{\partial\bar{u}_w}{\partial t}=-\mathrm{div}(\vec{q})+S_r\frac{\partial\varepsilon_v}{\partial t} \quad , \tag{13}$$

where $\mu=\partial S_r/\partial\bar{u}_w$. The mass flux of pore water can be defined by Darcy's Law as

$$\vec{q}=-k\,\mathrm{grad}(h) \quad , \tag{14a}$$

where $h=u_w/\rho_w g+z$ is water head and ρ_w is the density of pore water. To unify the variables, rewrite Eq. (14a) to following format:

$$\vec{q}=-\bar{k}\,\mathrm{grad}(\bar{h}) \quad , \tag{14b}$$

where $\bar{h}=\bar{u}_w/\rho_w g+z$. The new coefficient of permeability $\bar{k}$ can be determined in the same way as the normal coefficient k. Substituting Eq. (14b) into Eq. (13) yields

$$\mu n\frac{\partial\bar{u}_w}{\partial t}=-\frac{\partial}{\partial r}\bar{k}_r\frac{\partial\bar{h}}{\partial r}-\frac{\bar{k}_r}{r}\frac{\partial\bar{h}}{\partial r}-\frac{\partial}{\partial z}\bar{k}_z\frac{\partial\bar{h}}{\partial z}+S_r\frac{\partial\varepsilon_v}{\partial t} \quad , \tag{15}$$

For a case like quasi saturated state, where the pore air is found to be enclosed in pore water in form of air bubbles, the pore air and pore water together can be treated as compressible fluid. The equations of mass flux of pore water can be expressed as

$$m_f n\frac{\partial u_w}{\partial t}=-\frac{\partial}{\partial r}k_r\frac{\partial h}{\partial r}-\frac{k_r}{r}\frac{\partial h}{\partial r}-\frac{\partial}{\partial z}k_z\frac{\partial h}{\partial z}+\frac{\partial\varepsilon_v}{\partial t} \quad , \tag{16}$$

where m_f is the compressible coefficient of pore fluid. If the degree of saturation close to 1, Eq. (15) can degenerate into Eq. (16) automatically by setting $\mu=m_f$.

2 Constitutive models

2.1 Double hardening elasto-plastic model for soil skeleton

The stresses mentioned in the following section all represent effective stresses. A double hardening elato-plastic model for saturated soils (SHEN Zhu-jiang[8], 1995) is introduced to cater for unsaturated soils. The yield function of the model is expressed as,

$$F(\sigma,\varepsilon_v^p,\varepsilon_s^p)=\frac{\sigma_m}{1-[\dfrac{\eta}{\alpha(\varepsilon_s^p)}]^n}-p(\varepsilon_v^p) \quad , \tag{17}$$

where $\eta=\frac{1}{\sqrt{2}}[(\frac{\sigma_1-\sigma_2}{\sigma_1+\sigma_2})^2+(\frac{\sigma_2-\sigma_3}{\sigma_2+\sigma_3})^2+(\frac{\sigma_3-\sigma_1}{\sigma_3+\sigma_1})^2]^{\frac{1}{2}}$. n is a power number greater than 1. When n = 1.2, the shape of yield surface is close to ellipse (see Fig. 1). p and α are the two hardening parameters which are functions of plastic volumetric strain ε_v^r and plastic shear strain ε_s^p in the following forms, respectively,

$$p=p_0\exp(\frac{\varepsilon_v^p}{c_c-c_e}) \quad , \tag{18}$$

$$\alpha=\alpha_m-(\alpha_m-\alpha_0)\exp(\frac{\varepsilon_s^p}{c_a}) \quad , \tag{19}$$

Eq. (18) is in the same form as Cambridge model. c_c and c_e are the virgin compression slope and rebound slope in ε_v - ln$p$ plot, respectively. In Eq. (19), $\alpha_m=\sqrt[n]{1+n}\sin\varphi$. φ is the residual angle of inner friction. α_0 and c_a are other two constants, which can be determined by

unloaded triaxial compression test in which axial load keep fixed and confining pressure to be reduced step by step. According to the traditional plastic theory, plastic strain increment is determined as

$$\{\Delta\varepsilon^{\mathrm{p}}\}=\frac{1}{H}\{\frac{\partial F}{\partial\sigma}\}\{\frac{\partial F}{\partial\sigma}\}^{\mathrm{T}}\{\Delta\sigma\} \quad , \tag{20}$$

Hardening modulus H can be calculated as

$$H=-\frac{\partial F}{\partial\alpha}\frac{\partial\alpha}{\partial\varepsilon_{\mathrm{s}}^{\mathrm{p}}}\frac{\partial F}{\partial\sigma_{\mathrm{s}}}-\frac{\partial F}{\partial p}\frac{\partial p}{\partial\varepsilon_{\mathrm{v}}^{\mathrm{p}}}\frac{\partial F}{\partial\sigma_{\mathrm{m}}} \quad , \tag{21}$$

where $\sigma_s=\frac{1}{\sqrt{2}}[(\sigma_1-\sigma_2)^2+(\sigma_2-\sigma_3)^2+(\sigma_3-\sigma_1)^2]^{\frac{1}{2}}$.

Stress paths for uniaxial compression and rebound procedure simulated by this model are illustrated in Fig. 1. Line *abc* represents elastic rebound. A subsequent yielding occurs when stress path reaches point *c* during unloading after crossing the horizontal axis, as illustrated in the figure. The sloping angle of initial tangent to newly yield surface is larger than those to the previous yield surfaces. $\sigma_3-\sigma_1$ relationships for loading and unloading are presented in Fig. 2. Not like Line *oabcd* which represents the double hardening model, along Line *oabcd'* - traditional single hardening model, the yield point only occurs when vertical stress becomes zero.

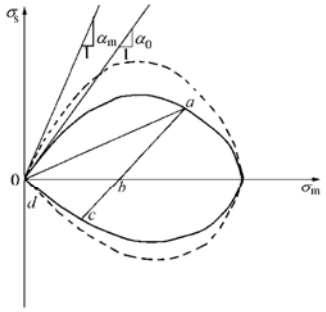

Fig. 1 Double hardening yield surfaces

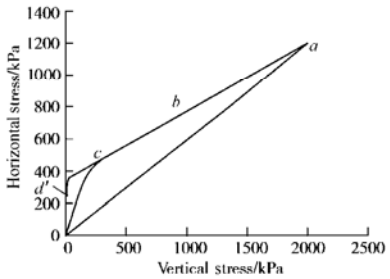

Fig. 2 Lateral pressure variations in uniaxial compression

2.2 Soil-water characteristic curve

If the stress-strain curves obtained from compression test and shrinkage test upon drying with the same initial condition are plotted in the same plan, compressive stress p corresponding to suction s can be determined as homologous effective suction $\bar{s}$ in terms of equivalent principle, as shown in Fig. 3. After obtaining $\bar{s}-s$ relationship, normal soil-water characteristic equation $S_{\mathrm{r}}=f(s)$ can be expressed in the form of $S_{\mathrm{r}}=f(\bar{s})$, as illustrated by dashed line in Fig. 4.

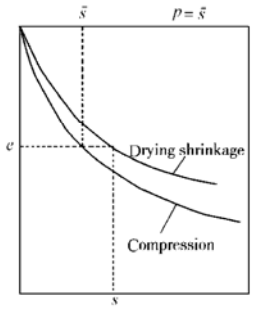

Fig. 3 Determination of effective suction

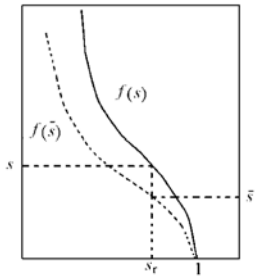

Fig. 4 Soil-water characteristic curves for effective suction

The soil-water characteristic curve can be divided into two segments in numerical computation. The degree of saturation is assumed to be 0.95 if suction is less than air entrance pressure s_{e}, where the soil can be treated as the quasi-saturated soil. If suction is greater than s_{e}, the degree of saturation can be determined by the following equation

$$S_{\mathrm{r}}=S_{\mathrm{r0}}+(0.95-S_{\mathrm{ro}})(\frac{\bar{s}}{s_{\mathrm{e}}})^{-m} \quad , \tag{22}$$

where S_{r0} is a parameter. Differentiating Eq. (22) by $\bar{s}$, it can be derived as (account for $\bar{s}=-\bar{u}_{\mathrm{w}}$)

$$\mu=(0.95-S_{\mathrm{ro}})\frac{m}{\bar{u}_{\mathrm{w}}}(\frac{-\bar{u}_{\mathrm{w}}}{s_e})^{-m} \quad , \tag{23}$$

where μ is a negative value.

2.3 Coefficient of permeability

If the relationships of k_{r} and k_{z} with suction s are obtained in laboratory, the relationships of $\bar{k}_{\mathrm{r}}$ and $\bar{k}_{\mathrm{z}}$ with $\bar{s}$ can also be established after suction s to be converted to equivalent suction $\bar{s}$. In the following computation, anisotropy of seepage is not taken into account, and the coefficient of permeability $\bar{k}$ is determined by the following empirical relationship:

$$\bar{k}=k_{\mathrm{s}}\exp(-c_{\mathrm{k}}\frac{\bar{s}-s_{\mathrm{e}}}{p_{\mathrm{a}}}) \quad , \tag{24}$$

where k_s is the coefficient of permeability of saturated soils. c_k is an empirical constant and p_a is the atmospheric pressure. Assuming $\bar{k} = k_s$, if $\bar{s} \le s_e$.

3 Computation methods

3.1 Finite element discretization

Isoparametric the elements are implemented with the same interpolating functions for both displacements and water head, i.e.,

$$\begin{Bmatrix} u_r \\ u_z \\ u_{m1} \end{Bmatrix} = \sum_{i=1}^{np} N_i \begin{Bmatrix} u_{ri} \\ u_{zi} \\ \bar{u}_{wi} \end{Bmatrix} \quad , \tag{25}$$

where *np* represents the number of nodes in one element, and u_{ri}, u_{zi} and $\bar{u}_{wi}$ are the three nodal variables at point *i*. Galerkin method is used to discretize Eqs. (10) and (15). Finite difference method is used for time domain discretization with formulation as

$$\int_{t_k}^{t_k+\Delta t} (\ )\,\mathrm{d}t = \Delta t[(1-\beta)(\ )_{t_k} + \beta(\ )_{t_k+\Delta t}] \quad , \tag{26}$$

where Δt is the time increment; $(\ )_{t_k}$ and $(\ )_{t_k+\Delta t}$ are the value of function at time t_k and $t_k + \Delta t$, respectively; β is a weight parameter. Therefore, finite element equations for node *i* (*i*=1, 2, ⋯, *Nt*) can be expressed as

$$\begin{cases} \sum_{j=1}^{Nt}[k_{ij}^{11}\Delta u_{rj} + k_{ij}^{12}\Delta u_{zj} + k_{ij}^{13}\Delta \bar{h}_j] = \Delta F_{ri} \quad , \\ \sum_{j=1}^{Nt}[k_{ij}^{21}\Delta u_{rj} + k_{ij}^{22}\Delta u_{zj} + k_{ij}^{23}\Delta \bar{h}_j] = \Delta F_{zi} \quad , \\ \sum_{j=1}^{Nt}[k_{ij}^{31}\Delta u_{rj} + k_{ij}^{32}\Delta u_{zj} + k_{ij}^{33}(\bar{h}_{j0} + \beta\Delta \bar{h}_j) + s_{ij}\Delta \bar{h}_j] = \Delta Q_i \quad , \end{cases} \tag{27}$$

where *Nt* represents the total number of nodes; ΔF_{ri}, ΔF_{zi} and ΔQ_i are the load increments and flux increment at node *i*, respectively; $\bar{h}_{i0}$ represents the water head value at node *i* at time t_k; the integral parameter $\beta = 2/3$ is adopted in present calculation. The elements of coefficient matrix in the finite element equations are expressed as follows:

$$k_{ij}^{11} = \int[d_{11}\frac{\partial N_i}{\partial r}\frac{\partial N_j}{\partial r} + d_{33}\frac{N_i}{r_i}\frac{N_j}{r_j} + d_{44}\frac{\partial N_i}{\partial z}\frac{\partial N_j}{\partial z} + d_{13}(\frac{N_i}{r_i}\frac{\partial N_j}{\partial r} + \frac{N_j}{r_j}\frac{\partial N_i}{\partial r}) + d_{14}(\frac{\partial N_i}{\partial r}\frac{\partial N_j}{\partial z} + \frac{\partial N_j}{\partial r}\frac{\partial N_i}{\partial z}) + d_{34}(\frac{N_i}{r_i}\frac{\partial N_j}{\partial z} + \frac{N_j}{r_j}\frac{\partial N_i}{\partial z})]2\pi r\,\mathrm{d}r\,\mathrm{d}z \quad , \tag{28a}$$

$$k_{ij}^{12} = \int[(d_{12}\frac{\partial N_i}{\partial r}\frac{\partial N_j}{\partial z} + d_{14}\frac{\partial N_i}{\partial r}\frac{\partial N_j}{\partial r} + d_{23}\frac{N_i}{r_i}\frac{\partial N_j}{\partial r} + d_{24}\frac{\partial N_i}{\partial z}\frac{\partial N_j}{\partial z} + d_{44}\frac{\partial N_j}{\partial r}\frac{\partial N_i}{\partial z} + d_{34}\frac{N_i}{r_i}\frac{\partial N_j}{\partial z}]2\pi r\,\mathrm{d}r\,\mathrm{d}z \quad , \tag{28b}$$

$$k_{ij}^{21} = \int[d_{12}\frac{\partial N_i}{\partial z}\frac{\partial N_j}{\partial r} + d_{14}\frac{\partial N_i}{\partial r}\frac{\partial N_j}{\partial r} + d_{23}\frac{N_j}{r_j}\frac{\partial N_i}{\partial z} + d_{24}\frac{\partial N_i}{\partial z}\frac{\partial N_j}{\partial z} + d_{44}\frac{\partial N_i}{\partial r}\frac{\partial N_j}{\partial r}) + d_{34}\frac{N_j}{r_j}\frac{\partial N_i}{\partial r}]2\pi r\,\mathrm{d}r\,\mathrm{d}z \quad , \tag{28c}$$

$$k_{ij}^{22} = \int[d_{22}\frac{\partial N_i}{\partial z}\frac{\partial N_j}{\partial z} + d_{44}\frac{\partial N_i}{\partial r}\frac{\partial N_j}{\partial r} + d_{24}(\frac{\partial N_i}{\partial z}\frac{\partial N_j}{\partial r} + \frac{\partial N_j}{\partial z}\frac{\partial N_i}{\partial r})]2\pi r\,\mathrm{d}r\,\mathrm{d}z \quad , \tag{28d}$$

$$k_{ij}^{33} = -\int[\bar{k}_r\frac{\partial N_i}{\partial r}\frac{\partial N_j}{\partial r} + \bar{k}_z\frac{\partial N_i}{\partial z}\frac{\partial N_j}{\partial z}]2\pi r\,\mathrm{d}r\,\mathrm{d}z \quad ,$$

$$k_{ij}^{13} = -\rho_w g\int(\frac{N_i}{r_i} + \frac{\partial N_i}{\partial r})N_j\,2\pi r\,\mathrm{d}r\,\mathrm{d}z \quad ,$$

$$k_{ij}^{23} = -\rho_w g\int\frac{\partial N_i}{\partial z}N_j\,2\pi r\,\mathrm{d}r\,\mathrm{d}z \quad ,$$

$$k_{ij}^{31} = -\rho_w g\int(\frac{N_j}{r_j} + \frac{\partial N_j}{\partial r})N_i\,2\pi r\,\mathrm{d}r\,\mathrm{d}z \quad ,$$

$$k_{ij}^{32} = -\rho_w g\int\frac{\partial N_j}{\partial z}N_i\,2\pi r\,\mathrm{d}r\,\mathrm{d}z \quad ,$$

$$s_{ij} = -\rho_w g\int[c_s N_i N_j]2\pi r\,\mathrm{d}r\,\mathrm{d}z \quad ,$$

where $c_s = m_r n$ (for saturated case) or $c_s = \mu n / S_r$ (for unsaturated case).

3.2 Boundary conditions

The computation domain is illustrated as zone *oabcd* in Fig. 5, where axis *z* represents the symmetrical axis, *oa* the radius and *cd* the ground surface. Groundwater table is assumed to be at *oa*, where both the nodal displacements and water head at this boundary are assumed to be zero. The ground surface *cd* is the boundary subjected to loading and evaporation.

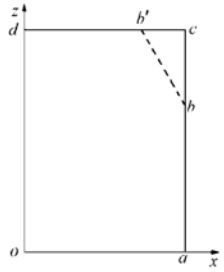

Fig. 5 Computation domain

3.3 Simulation of cracking

The horizontal displacements on *abc* plane are prohibited before crack to be formed. During the evaporating, tensile stress in horizontal direction will be developed gradually. Crack at a point is assumed to occur if the tensile stress in horizontal direction at that point fulfills the following requirement as

$$-\sigma_r = p_t \quad , \tag{29}$$

where p_t is the tensile strength of soil. The tensile strength will be expressed in total stress. The effective stress induced by suction only has effect on shear deformation, but not on tensile strength.

Once horizontal stress at one node reaches the tensile strength as defined in Eq. (29), the freedom of horizontal displacement has to be assigned to the node, and an increment of force equals to tensile force will have to be applied to the node on the vertical surface of the crack in a reverse direction to tension force. Once the cracked section becomes free face, evaporation will take place on that surface. Horizontal stress of other nodes at the bottom of the cracked section will progressively increase to reach the tensile strength. Therefore, these bottom nodes will separate from one and another eventually. The propagation of crack will therefore be restrained if the crack moves near the groundwater table.

4 Computation examples

4.1 Computation parameters

The sensitivities of computation parameters to spacing and depth of cracks will be investigated in the following computation examples. Computation parameters are divided into two groups.

In the first group the parameters have fixed value: wet density $\rho = 0.002$ kg/cm^3, lateral stress coefficient $k_0 = 0.6$, Poisson's ratio $\nu = 0.3$, initial void ratio $e_0 = 1.0$, coefficient of permeability for saturated soils k_s=1.0×10^{-5} cm/s, $\alpha_m = 1.0$, $\alpha_0 = 0.75$, $c_a = 0.05$, $s_e = 20$ kPa, $S_{r0} = 0.2$.

In the second group the parameters take three different values: $c_c = 0.03, 0.06, 0.12$; $m = 0.6, 0.4, 0.2$; $p_t = 5, 10, 15$ kPa. The value of c_e is 1/6 of c_c. The soil-water characteristic curves for different values of m are illustrated in Fig. 6.

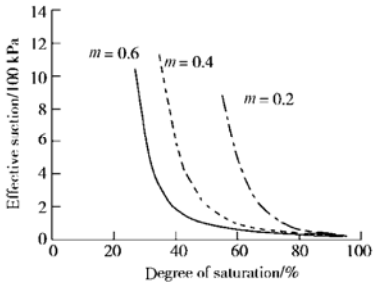

Fig. 6 Soil-water characteristic curves with different values of m

Based on the above-given parameters, computations for normally consolidated clays have been carried out. A typical finite element mesh of the computed examples is illustrated in Fig. 7. Three schemes of computation with different domain size have been executed, with the radius of the domain assumed to be 10, 20 and 30 cm and a fixed depth of 200 cm.

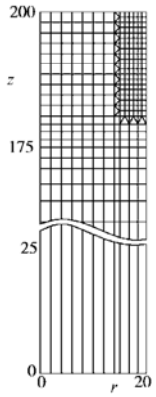

Fig. 7 Finite element mesh

4.2 Computations results

In this computation, the soil in computation domain is assumed to be saturated normally consolidated clay. It desiccates gradually at an evaporation rate of 1mm/d, meanwhile shrinkage cracks will develop. Total 45 cases have been simulated. For most of cases, the time duration is assumed to be 30 d except for one case where the time duration is assumed to be 90 d. The computation results for all the cases on the 30th day after evaporation starts are presented in Table 1. Assuming the spacing of cracks given in the table is double of the radius of computation zone. The computed results show that, the maximum width of cracks is 1.78 cm, the maximum depth of cracks 28.0 cm, the maximum settlement on ground surface 3.86 cm. and the maximum suction at the center of ground surface 49.7 kPa. Of course, this suction value is related to the so-called reduced suction, which is less than the true suction.

According to the computed results, the two factors which have significant effect on the width of cracks are the compressibility of soils and the spacing of cracks. In other words, the larger the compressibility and spacing are, the larger the width of the cracks is be. Certainly tensile strength has effect on the width of cracks too. There are no cracks in all cases with $p_t = 15$ kPa until the 30th day.

The two factors which affect the depth of cracks

Table 1 Computed results of soil cracking using variable parameters

spacing	tensile strength/kPa	5			10									15		
	suction parameter m	0.4			0.6			0.4			0.2			0.4		
of cracks /cm	compressibility C_c	0.03	0.06	0.12	0.03	0.06	0.12	0.03	0.06	0.12	0.03	0.06	0.12	0.03	0.06	0.12
20	surface settlement/cm	1.34	2.25	3.39	0.97	1.67	2.64	1.18	2.02	3.08	1.61	2.70	3.84	1.18	2.02	3.07
	Surface suction/kPa	46.4	43.3	39.1	37.5	36.1	34.2	41.3	39.1	36.2	49.3	45.0	39.6	41.2	39.0	36.2
	depth of caracks/cm	28.0	28.0	21.5	1.0	1.0	1.0	5.0	5.0	5.0	13.0	13.0	9.0	0	0	0
	width of cracks/cm	0.12	0.22	0.38	0.02	0.04	0.09	0.03	0.06	0.11	10.05	0.09	0.15	0	0	0
40	Surface settlement/cm	1.27	2.13	3.24	0.97	1.67	2.63	1.18	2.03	3.08	1.63	2.72	3.86	1.18	2.02	3.07
	surface suction/kPa	43.9	41.0	37.5	37.5	36.1	34.2	41.2	39.0	36.2	49.7	45.1	39.7	41.2	39.0	36.2
	depth of caracks/cm	28.0	24.5	21.5	1.0	1.0	1.0	5.0	5.0	5.0	13.0	13.0	9.0	0	0	0
	width of cracks/cm	0.22	0.38	0.66	0.02	0.05	0.10	0.03	0.07	0.13	0.07	0.13	0.21	0	0	0
60	surface settlement/cm	1.24	2.10	3.20	0.97	1.67	2.63	1.18	2.02	3.08	1.63	2.71	3.86	1.18	2.02	3.07
	surface suction/kPa	42.9	40.3	36.9	37.5	36.1	34.2	41.2	39.0	36.2	49.5	44.9	39.6	41.2	39.0	36.2
	depth of caracks/cm	28.0	24.5	24.5	1.0	1.0	1.0	5.0	5.0	5.0	13.0	13.0	9.0	0	0	0
	width of cracks/cm	0.29	0.52	0.89	0.02	0.05	0.10	0.03	0.07	0.13	0.08	0.15	0.23	0	0	0

mostly are the tensile strength of soils and the compressibility, viz. the cracks will be deeper in soil with lower tensile strength and lower compressibility. The reason why the cracks will be deeper in soils with lower compressibility is because the soil with higher modulus of compressibility is more brittle and sensitive to tensile stress. The suction parameter m does also play an import role in the development of cracks. It is because that with the same degree of saturation, the suction will tend to be larger if value of m becomes smaller. As a result, the cracks will therefore develop deeper and wider. Although value of m does have more effect on the suction on ground surface than any other parameters, the suction on ground surface would actually not be over-influenced as shown in Fig. 8. It is because that the degree of saturation would increase if the value of m decreases. Similarly, the effect of value of m on vertical displacement at center and horizontal displacement at edge should also not that significant as illustrated in Fig. 9.

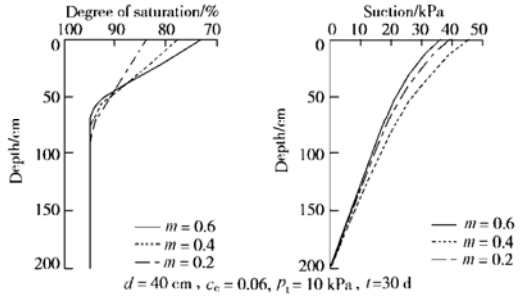

Fig. 8 Profiles of calculated suction and degree of saturation at the centre line for different values of *m*

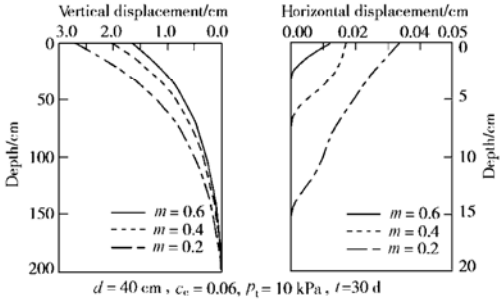

Fig. 9 Distribution of calculated displacement at the edge of computation domain for different values of *m*

A computation of evaporation over 90 d has also been carried out as one of many cases with the computation results presented in Fig. 10, Fig. 11 and Fig. 12. In view of the results of analysis (Fig. 10), the suction would increase gradually corresponding to a decrease in the degree of saturation with time. Based on the calculated displacement of crack edge (Fig. 11), crack should become deeper and wider continuously companying with the shrinkage of soil. By the way, the plot of crack width versus depth does not turn into an expected smooth curve with an explanation given as that the number of the nodes where crack occurs does vary with the increase of evaporation capacity. Within one step of time, occasionally crack occurs at only one node but sometimes at several nodes. A detailed illustration on the development of the settlement and the crack width as well as the degree of saturation and the suction is presented in Fig. 12.

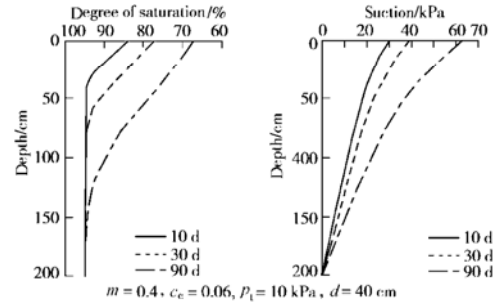

Fig. 10 Profiles of calculated suction and degree of saturation at the centre line at different elapsed time

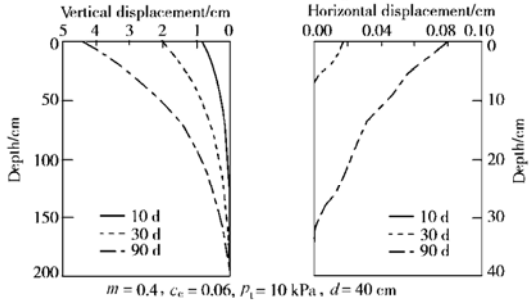

Fig. 11 Distribution of calculated displacement at the edge of computation domain at different elapsed time

The development of crack may also be influenced by many other factors, such as wetting-drying cycle, temperature cycle and soil heterogeneity, especially the uneven distribution of tensile strength. Therefore, the aforementioned computation method may still need to be further improved for more precise simulation of the actual problems.

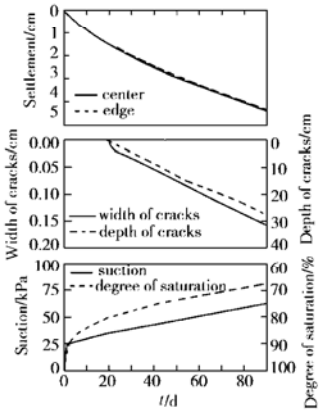

Fig. 12 Evolution of calculated variables with time

5 Conclusions

The mechanical properties of soil are significantly affected by confining pressures with big variation. Therefore the soil is a sort of heterogeneous material in nature. It is difficult to simulate the cracking process in the soils by using the fracture mechanics which is proposed on the basis of homogeneous medium concept. The cracking of soils is controlled by tensile strength. Based on the criterion of tensile failure, finite element method or other numerical methods can be implemented to trace the propagation of cracks.

Once soil starts cracking, pore air can easily escape. Hence, the simplified consolidation theory of unsaturated soils based on the assumption that pore air pressure equals to the atmospheric pressure can be adopted in order to simulate the generation and propagation of cracks upon evaporation. In this theory, a variable named reduced suction or equivalent suction is used. The governing equations of simplified consolidation theory are formally same as those of consolidation problem of saturated soils. Therefore, no much effort is required to amend the existing finite element programs for saturated soil to fit with the present analysis.

In this paper, the distribution of irregular polygonal crack has been simplified to an axisymmetric problem with a double hardening elasto-plastic model adopted for soil skeleton. The sensitivities of parameters to width and depth of cracks have been studied. Total 45 cases with various different combinations of parameters have also been investigated. According to the computed results, besides the tensile strength, the most significant factor which affects the width and depth of cracks, is the compressibility of soils.

References:

[1] MORRIS P H, GRAHAM J, WILLIAM D J. Cracking in drying soils [J], Canadian Geotechnical Journal, 1992, **29**: 263 – 277.

[2] ABU-HEJLEH A N, ZNIDARCIC D. Desiccation theory for soft cohesive soils [J], Journal of Geotechnical Engineering, ASCE, 1995, **121**(6): 493 – 502.

[3] KONRAD J M, AYAD R. An idealized framework for the analysis of cohesive soils undergoing desiccation [J]. Canadian Geotechical Journal, 1997, **34**: 477 – 488.

[4] LEE F H, LO K W, LEE S L. Tension crack development in soils [J]. Journal of Geotechnical Engineering, ASCE, 1998, **114**(8): 915 – 929.

[5] LI Hong-sheng, ZHU Yuan-lin. Fracture mechanics of frozen soil and its application [M]. Beijing: Ocean Press, 2002.

[6] SHEN Z J. Reduced suction and simplified consolidation theory for expansive soils[C]// Proceedings of First International Conference on Unsaturated soils. Paris, 1996.

[7] JIANG Peng-nian. On the engineering properties of unsaturated soils [J]. Chinese Journal of Geotechnical Engineering, 1989, **11**(6): 39 – 59.

[8] SHEN Zhu-jiang. A double hardening model for clays [J]. Rock and Soil Mechanics, 1995, **16**(1): 1 – 8.